COMPUTATIONAL ANALYSIS OF TRANSIENT TURBULENT FLOW AND CONJUGATE HEAT TRANSFER CHARACTERISTICS IN A SOLAR COLLECTOR PANEL WITH INTERNAL, RECTANGULAR FINS AND BAFFLES

by

Rachid SAIM [a*], ***Said ABBOUDI*** [b], ***and Boumédiène BENYOUCEF*** [c]

[a] Département de Génie Mécanique, Faculté des Sciences de l'Ingénieur, Université Abou Bekr Belkaid, Tlemcen, Algérie
[b] Laboratoire Systémes et Transports (SET), UTBM, Site de Sévenans, France
[c] Unité de Recherche des Matériaux et Energies Renouvelables (URMER), Faculté des Sciences, Université Abou Bekr Belkaid, Tlemcen, Algérie

Original scientific paper
UDC: 621.383.51:532.517.4
DOI: 10.2298/TSCI1001221S

The poor thermal exchange between the absorber and the fluid in the solar air flat plate collector, gives the bad performance and the mediocre thermal efficiency. The introduction of obstacles in the dynamic air vein of the solar collector in order to obtain a turbulent flow is a technique that improves the thermal exchange by convection between the air and the absorber. This article present a computational analysis on the turbulent flow and heat transfer in solar air collector with rectangular plate fins absorber and baffles which are arranged on the bottom and top channel walls in a periodically staggered way. To this end we solved numerically, by the finite volumes method, the conservation equations of mass, momentum and energy. The low Reynolds number k-ε model was adopted for the taking into account of turbulence. The velocity and pressure terms of momentum equations are solved by the SIMPLE algorithm. The parameters studied include the entrance mass flow rate of air. The influence of the mass flow rate of air on the axial velocity and the efficiency of upward type baffled solar air heaters have been investigated numerically. The results show that the flow and the heat transfer characteristics are strongly dependent on mass-flow rate of air and the presence and/or the absence of the baffles and fins in the solar collector. It was observed that increasing the Reynolds number will increase the efficiency of the solar panel, as expected.

Key words: *baffle, solar collector, forced convection, fins, turbulent flow, low Reynolds number*

Introduction

In the solar energy possesses, a thermal conversion mode necessitates a simple technology which is adapted to the site and to the particular region for many applications. These sys-

* Corresponding author; e-mail: saimrachid@yahoo.fr

tems are all based on the solar air flat plate collector. The air is a bad conductor of heat on the basis of its low proprieties used in the solar collectors. The user is obliged to employ a fully developed turbulent flow for air. Among the methods used to increase the thermal heat transfer between the absorber-plate and the fluid is the insertion of the obstacles arranged into the air channel duct. These obstacles allow a good distribution of the fluid flow. The fluid flow and heat transfer characteristics over baffles and fins has been studied by different authors. The presence of these baffles causes the flow to separate, reattach and create reverse flow (Yang *et al*. [1], Patankar *et al.* [2], and Kelkar *et al.* [3]). In general, Nusselt number and friction coefficient increase with the Reynolds number (Berner *et al*. [4], Webb *et al.* [5], and Lopez. *et al.* [6]). Cheng *et al.* [7] have investigated the case where the transverse baffles are not symmetrically placed. Their results have indicated that the relative position of the baffle arrays is an influential factor on the flow field, especially for baffles with a large height. In the experimental efforts, Founti *et al.* [8] used LDA to deduce the velocity field in an axisymmetric heat exchanger with baffles on the shell-side surface. The similar distributions of the mean flow velocity and turbulent intensity were found after two sets of baffles from the channel entrance. Later, Berner *et al*. [9] and Berner *et al.* [10] obtained experimental results of mean velocity and turbulence distributions in flow around segmented baffles. Experimental investigation of characteristics of the turbulent flow and heat transfer inside the periodic cell formed between segmented baffles staggered in a rectangular duct was studied by Habib *et al.* [11]. The experimental results indicated that the pressure loss increased as the baffle height did. For a given flow rate, local and average heat transfer parameters increase with increasing Reynolds number and baffle height. Recently, Bazdid-Tehrani *et al.* [12] have presented a numerical solution for the fluid flow and heat transfer in a duct with in line baffles and reported that the heat transfer behavior of this type of baffles is somewhat inefficient for large values of the blockage ratio. However, as noted by previous articles, for the case of staggered baffles, the opposite is true. Ackermann *et al.* [13] presented a computational study to examine the fully developed laminar flow and heat transfer characteristics in solar collector panels with internal, longitudinal, corrugated fins. The fins are integrally attached to the upper and lower panel walls. The objective of the study is to determine the effects of varying the fin pitch, the fin thickness, the ratio of the thermal conductivity of the panel walls and the fin to that of the fluid, and the thermal boundary condition on the panel heat transfer and pressure drop.

The particularity of this computational study is the conjugate heat transfer aspect. In the first part of this paper, we present a hydrodynamic aspect and the influence of the air mass flow rates on the velocities. In the second part the analysis of temperature profile of the absorber, the insulator, and the air was presented. The comparison of the efficiency between the solar air heaters with and without fins and baffles has been investigated numerically.

Problem statement

One of elements treated in the specialized literature (Bhargava *et al.* [14]; Wijeysundera *et al.* [15]) is the manner of air circulation towards the absorber. Various configurations are possible and the main generic types are shown schematically in fig. 1.

As the experimental work done by Ben Slama [see 27], the solar collector type 2 in fig. 1, equipped with baffles, is better than type 4 because it provides significant thermal advantages over those without baffles.

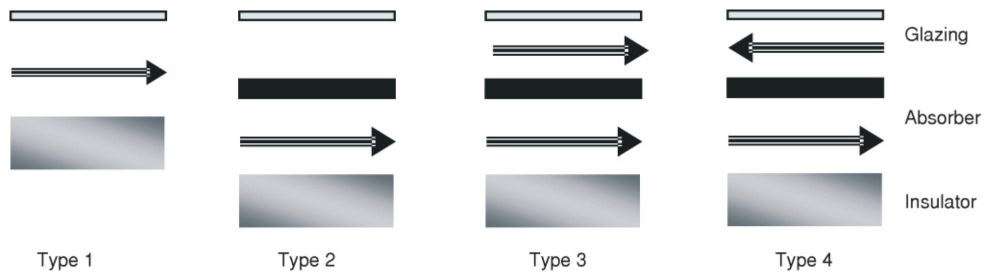

Figure 1.Various configurations of air passage in solar collector panel

Our problem is integrated in the air solar collector with baffles plate and fins. Figure 2 presents the upward type solar air heater under consideration. The physical domain is between two parallel plates. The outer surface of the top wall of the channel is uniformly heated while the outer surface of the bottom wall is thermally insulated. The fluid is incompressible with constant properties and the flow is considered turbulent and unsteady.

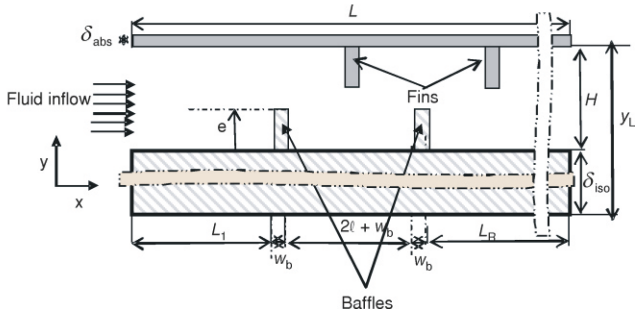

Figure 2. Schematic of the problem

Mathematical formulation

Youcef-Ali [16], Youcef-Ali [17], and Moummi *et al.* [18] have shown that the low thermophysical characteristics of air used as a heat transfer fluid in the solar collectors with thermal conversion require a fully developed turbulent flow.

Governing equations

The k-ε, low-Reynolds number closure model proposed by Jones *et al.* [19] is adopted in this study. In Cartesian co-ordinate, the continuity, momentum, energy, and turbulence equations for unsteady incompressible flows can be written as:

Continuity equation

$$\frac{\partial \rho}{\partial t} \quad \frac{\partial u}{\partial x} \quad \frac{\partial (\rho v)}{\partial y} \quad 0 \tag{1}$$

x-Momentum equation:

$$\rho \frac{\partial u}{\partial t} \quad \rho u \frac{\partial u}{\partial x} \quad \rho v \frac{\partial u}{\partial y} \quad \frac{\partial p}{\partial x} \quad \frac{\partial}{\partial x} (\mu \quad \mu_t) 2 \frac{\partial u}{\partial x} \quad \frac{\partial}{\partial y} (\mu \quad \mu_t \quad \frac{\partial u}{\partial y} \quad \frac{\partial v}{\partial x} \tag{2}$$

y-Momentum equation

$$\rho\frac{\partial v}{\partial t}+\rho u\frac{\partial v}{\partial x}+\rho v\frac{\partial v}{\partial y}=-\frac{\partial p}{\partial y}+\frac{\partial}{\partial y}\left[(\mu+\mu_t)2\frac{\partial v}{\partial y}\right]+\frac{\partial}{\partial x}\left[(\mu+\mu_t)\left(\frac{\partial u}{\partial y}+\frac{\partial v}{\partial x}\right)\right] \tag{3}$$

Turbulent energy equation

$$\rho\frac{\partial k}{\partial t}+\rho u\frac{\partial k}{\partial x}+\rho v\frac{\partial k}{\partial y}=\frac{\partial}{\partial x}\left[\left(\mu+\frac{\mu_t}{\sigma_\mathrm{k}}\right)\frac{\partial k}{\partial x}\right]+\frac{\partial}{\partial y}\left[\left(\mu+\frac{\mu_t}{\sigma_\mathrm{k}}\right)\frac{\partial k}{\partial y}\right]+P_\mathrm{k}-\rho\varepsilon-D \tag{4}$$

Turbulent dissipation equation

$$\begin{aligned}\rho\frac{\partial \varepsilon}{\partial t}+\rho u\frac{\partial \varepsilon}{\partial x}+\rho v\frac{\partial \varepsilon}{\partial y}&=\frac{\partial}{\partial x}\left[\left(\mu+\frac{\mu_t}{\sigma_\varepsilon}\right)\frac{\partial \varepsilon}{\partial x}\right]+\\&+\frac{\partial}{\partial y}\left[\left(\mu+\frac{\mu_t}{\sigma_\varepsilon}\right)\frac{\partial \varepsilon}{\partial y}\right]+(C_{\varepsilon1}f_1P_k-\rho C_{\varepsilon2}f_2\varepsilon)\frac{\varepsilon}{k}+E_\mathrm{LRN}\end{aligned} \tag{5}$$

Energy equation in the fluid region

$$\rho\frac{\partial T}{\partial t}+\rho u\frac{\partial T}{\partial x}+\rho v\frac{\partial T}{\partial y}=\frac{\partial}{\partial x}\left[\left(\frac{\mu}{\mathrm{Pr}}+\frac{\mu_\mathrm{t}}{\sigma_\mathrm{T}}\right)\frac{\partial T}{\partial x}\right]+\frac{\partial}{\partial y}\left[\left(\frac{\mu}{\mathrm{Pr}}+\frac{\mu_\mathrm{t}}{\sigma_\mathrm{T}}\right)\frac{\partial T}{\partial y}\right] \tag{6}$$

Energy equation in the solid region

$$\rho_\mathrm{s}C_\mathrm{ps}\frac{\partial T}{\partial t}=\lambda_\mathrm{s}\left(\frac{\partial^2 T}{\partial x^2}+\frac{\partial^2 T}{\partial y^2}\right) \tag{7}$$

For a two-dimensional flow production term becomes:

$$P_\mathrm{k}=\mu_\mathrm{t}\left\{2\left(\frac{\partial u}{\partial x}\right)^2+2\left(\frac{\partial v}{\partial y}\right)^2+\left(\frac{\partial v}{\partial x}+\frac{\partial u}{\partial y}\right)^2\right\} \tag{8}$$

The turbulent viscosity is calculated as:

$$\mu_\mathrm{t}=f_\mu\rho C_\mu\frac{k^2}{\varepsilon} \tag{9}$$

E_LRN is a term applied for the k-ε low Reynolds number model. The constants of the standard k-ε model are those given by Jones *et al.* [19] and are: $C_\mu = 0.09$, $C_{1\varepsilon} = 1.44$, $C_{2\varepsilon} = 1.92$, $\sigma_\mathrm{k} = 1$, $\sigma_\varepsilon = 1.3$, and $\sigma_\mathrm{t} = 0.9$.

In eqs. (4) and (5) the terms D and E_LRN are defined by:

$$D=2\mu\left[\left(\frac{\partial\sqrt{k}}{\partial x}\right)^2+\left(\frac{\partial\sqrt{k}}{\partial y}\right)^2\right]\quad\text{and}\quad E_\mathrm{LRN}=2\mu\frac{\mu_\mathrm{t}}{\rho}\left[\left(\frac{\partial^2 u}{\partial y^2}\right)^2+\left(\frac{\partial^2 v}{\partial x^2}\right)^2\right] \tag{10}$$

Low Reynolds number k-ε model

In the version of Versteeg *et al.* [20], the modelling damping functions f_1, f_2, and f_μ used for the LRN k-ε model are presented as:

$$f_\mu = (1 - \mathrm{e}^{-0.0165 R_\mathrm{y}})^2 \left(1 + \frac{20.5}{R_\mathrm{T}}\right) \tag{11}$$

$$f_1 = 1 + \left(\frac{0.05}{f_\mu}\right)^3 \tag{12}$$

$$f_2 = 1 - \mathrm{e}^{-R_T^2} \tag{13}$$

where

$$R_\mathrm{T} = \frac{\rho k^2}{\varepsilon\mu} \quad \text{and} \quad R_\mathrm{y} = \frac{\rho\sqrt{k}\,y}{\mu} \tag{14}$$

The damping function (f_μ), which is a function of dimensionless wall-normal distance $R_\mathrm{y} = y^+ = y(k)^{1/2}/\nu$, is used to model the damping effect associated with pressure-strain correlations in the vicinity of walls.

Boundary conditions

The computational domain and boundaries are presented as:

Inlet boundary: (x = 0)

The characteristic length is the equivalent diameter of the duct:

$$D_\mathrm{e} = \frac{4HB}{2(B + H)} \tag{15}$$

For the fluid region: $d_\mathrm{isol} \leq y \leq H + d_\mathrm{isol}$. The air is taken at ambient conditions:

$$\begin{aligned} u &= U_\mathrm{in} = \frac{4m}{\rho\pi D_\mathrm{e}^2} \\ v &= 0 \\ T &= T_\mathrm{in} \\ k_\mathrm{in} &= 0.005 U_\mathrm{in}^2 \\ \varepsilon_\mathrm{in} &= 0.1\sqrt{k_\mathrm{in}^3} \end{aligned} \tag{16}$$

where k_in is the inlet condition for the turbulent kinetic energy and ε_in – the inlet condition for the dissipation rate.

Exit boundary: (x = L),

For the fluid region: $d_\mathrm{isol} \leq y \leq H + d_\mathrm{isol}$, all gradients are assumed to be zero.

$$\frac{\partial\phi(L, y)}{\partial x} = 0 \tag{17}$$

where $\phi = (u, v, T, k, \varepsilon)$.

Wall side at the inlet and the exit solar collector for the solid region (absorber or insulator): $0 < y < d_{\mathrm{isol}}$ and $H + d_{\mathrm{isol}} \leq y < y_L$

$$\phi(0, y) = \phi(L, y) = 0 \quad \text{and} \quad \frac{\partial T_S(0, y)}{\partial x} = \frac{\partial T_S(L, y)}{\partial x} = 0 \tag{18}$$

where $\phi = (u, v, k, \varepsilon)$

Fluid solid interface: $u = v = 0$, $k = \varepsilon = 0$,

$$T_{\mathrm{f}} = T_{\mathrm{s}}, \; \lambda_f \left.\frac{\partial T_{\mathrm{f}}}{\partial n}\right|_{\mathrm{n}} = \lambda_{\mathrm{s}} \left.\frac{\partial T_{\mathrm{s}}}{\partial n}\right|_{\mathrm{n}} \tag{19}$$

where n is the coordinate normal to the wall.

The outer surface of the insulator: $y = 0$

we have:
$$\lambda_{\mathrm{isol}} \left.\frac{\partial T}{\partial y}\right|_{y=0} = h_{\mathrm{w}} [T(i, y = 0) - T_{\mathrm{a}}] \tag{20}$$

where T_{a} is the ambient temperature and h_{w} – the external convective heat transfer coefficient between air and glass cover. h_{w} depends primarily on the wind velocity V [21]:

$$h_{\mathrm{w}} = 5.7 + 3.8V \tag{21}$$

The top surface of the absorber: $y = H + d_{\mathrm{isol}} + d_{\mathrm{absor}}$

$$\lambda_{\mathrm{s\,absor}} \left.\frac{\partial T}{\partial y}\right|_{y=(H+\delta_{\mathrm{isol}}+\delta_{\mathrm{absor}})} = G_{\mathrm{v}} \tag{22}$$

where G_{v} is the incident solar radiation after glazing. This value is estimated for the site of Tlemcen town, Algeria, taken from ref. [22]

Collector efficiency

According to the mass flow rate of air, of the specific heat and the exit and the inlet temperatures of the air, Whillier [23], Hottel *et al*. [24], and Whillier [25] have presented the efficiency for sheet and tube solar energy collectors as:

$$\eta = \frac{Q_{\mathrm{u}}}{A_{\mathrm{c}} I_0} = \frac{mCp(T_{\mathrm{out}} - T_{\mathrm{in}})}{I_0 A_{\mathrm{c}}} \tag{23}$$

Although there are many different designs of flat plate collectors available, it is fortunately not necessary to develop a new analysis for each situation according to Hottel *et al.* [24].

Numerical solution procedure

A finite volume method was used to discretize the governing equations and boundary conditions. The numerical solution was obtained using the SIMPLE algorithm developed by Patankar [26]. The discrete conservation equations were solved by the TDMA and the line-by-line iterative methods proposed by Patankar [26]. The under-relaxation factor was carefully chosen to prevent large variations in the source terms.

Non-uniform grids are taken in both the fluid, baffles, and fins regions. For the conditions $m = 60$ kg/h, $L/B = 1.8/0.3 = 6$, $I_0 = 1043$ W/m^2, $w = 2$ cm, $\ell = 16$ cm, the effect of the grid size on efficiency and mean axial velocity was tested for various non-uniform grid systems ((106; 67), (112; 67), (118; 67), (112; 61), (112; 73) and (112; 80)) and the choice of the grid distribution (112; 67) was sufficient to provide a grid-independent. Typically, it took about 1500-2500 iterations to reach convergence.

Increasing the number of nodes up to (112; 117) does not affect much on the mean axial velocity. The minimum relative error defined by $Er = (\phi_{\text{grid1}} - \phi_{\text{grid2}})/\phi_{\text{grid1}}$ between the solutions of different grid studied is about 0.707% for efficiency of solar collector and less than 0.1559% for the mean axial velocity.

Code validation

The numerical code developed in the present work was tested against previous studies for turbulent flow over baffles and fins of solar collector. The heat transfer results are presented in terms of efficiency has been validated using the results of Ben Slama *et al*. [27]. They have numerically investigated a similar problem for air flow in a two dimensional channel for the following conditions (L/B = 1/6, I_0 = 830 W/m^2, w = 2 cm, ℓ = 8 cm). Figure 3 shows the efficiency of the solar collector against the volume flow rate of air, for unit area. This figure presents a good agreement between our results and those of Ben Slama *et al*. [27]. These slight differences between the two results are caused basically for three orders of reasons:

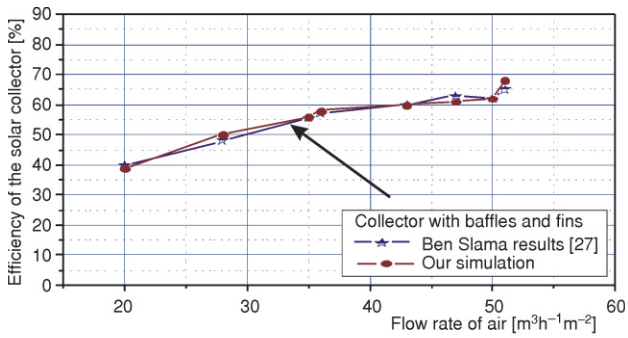

Figure 3. Comparison of our results in terms of efficiency with those of Ben Slama *et al.* [27] (L/B = 1/6, I_0 = 830 W/m^2, w = 2 cm, ℓ = 8 cm)

(1) Interaction of the solar collector with the medium which surrounds it: outside environment and the accessories and components of the thermal system which the solar collector is connected.
(2) Multiplicity of the phenomena of heat transfer concerned and the uncertainty of the experiment boundary conditions of problem.
(3) Occurrence of the turbulent phenomena associated with the convective movements which are established inside the solar collector.

Results and discussion

In order to better analyze the effects of the parameters under consideration, the following values are used in the numerical simulations.

Geometrical parameters: $Ac = BL = 0.54$ m^2; $L = 0.9$ m; $B = 0.6$ m; $H = 5.5$ cm; $w_b = 6$ cm, $\ell = 8$ and 16 cm. The absorber is made of aluminum ($\lambda_{absor} = 200$ Wm/K) and the insulator of polystyrene ($\lambda_{iso} = 0.034$ Wm/K).

Boundary conditions: $I_0 = 1043$ W/m^2; $T_a = 303.15$ K; $T_{f\,in} = 303.15$ K, $V = 1$ m/s.

The mass flow rate of air varies from 30 to 80 kg per hour. The air properties are used to evaluate the efficiency of the solar collector according to Latif [28].

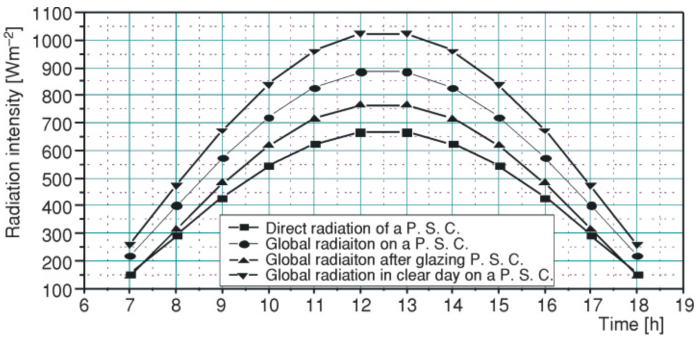

Figure 4. Evolution of total radiation (day of June for Tlemcen town (Algeria) [22]

In fig. 4, we present the different solar radiation for the town of Tlemcen on June 21 namely: direct global radiation, the constant radiation in a clear day, and finally the global radiation after glazing in plate solar collector including and taking into account the astronomical conditions of Tlemcen town.

For all calculations worked out in this article takes a regular form and reaches a maximum value of (1043 W/m^2) for the town of Tlemcen at solar midday [22] (fig. 4).

Hydrodynamics aspects

The impact of the baffle and fins on the structure of the near wall flow is presented in fig. 5 for the axial velocity of the air for $m = 30$ kg/h, L/B = 6, $I_0 = 1043$ W/m^2, $w = 2$ cm, $\ell = 8$ cm. A clockwise vortex is generated upstream near the first baffle. As the fluid turns upward into the by-pass passage between the top face of the first baffle and the upper channel wall, the fluid directly impinges the top face of the first fin causing a recirculation zone to be formed within the inter baffle and fin groove. The second important vortex is shown near the top of the domain in the downward region; it is caused by the accelerated flow between the tip of the first fin and the insulator. A third and more important clockwise vortex is also created downstream of the last fin.

Figure 6 shows the velocity profiles between the first baffle and the first fins at a position $x = 0.201$ m, $x = 0.232$ m, and $x = 0.241$ m from the entrance. The flow is characterized by the very

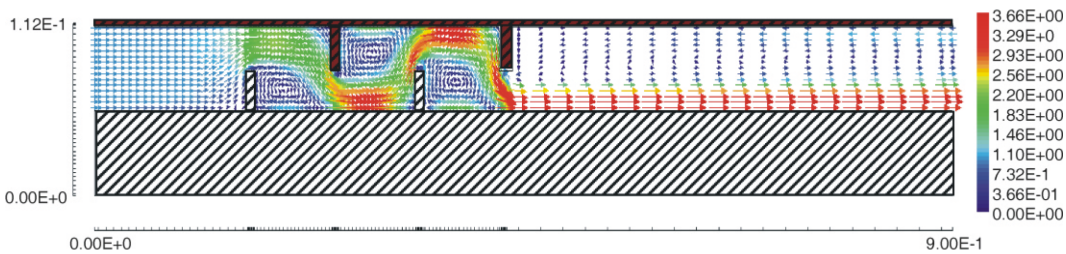

Figure 5. Axial velocity [ms^{-1}] field distribution in the solar collector (color image see on our web site)

high velocities at the lower part of the channel, approaching 250% of the reference velocity. In the upper part of the channel, negative velocities indicate the presence of the recirculation behind the first baffle. Its velocity is reduced in the upper part of the channel, while in the lower part is increased. The velocity profiles is almost flat in the lower part of the channel, while in the upper part the flow starts to accelerate toward the gap above the first fin.

In fig. 7, the velocity profiles between the first fin and the second baffle were presented at the positions: $x = 0.258$ m, $x = 0.29$ m, and $x = 0.314$ m from the entrance. Conversely with the preceding case, its velocity is reduced in the lower part of the channel and is increased in the upper part. The presence of the negative values of the velocity indicates that the flow starts to accelerate toward the gap above the second baffle.

The effect of the mass flow rate of air on the axial velocity profiles, in different sections of the solar collector, is shown in figs. 8-10. One observes that the flow accelerates in the direction of the flow and the length of the recirculation regions is proportional to the increase in the flow of air in flow. This result can be explain by the fact of the velocity increases of air flow and also the convective heat trans-

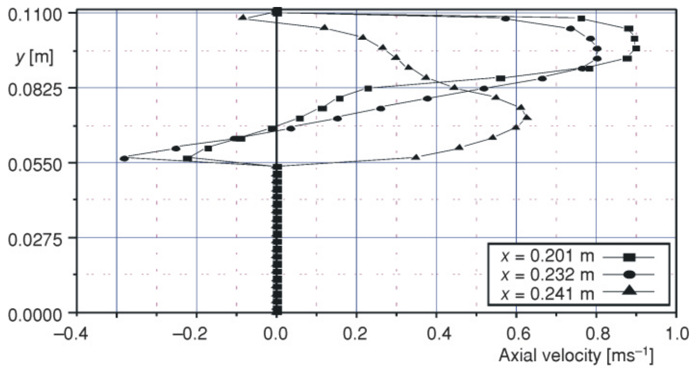

Figure 6. Velocity profiles between the first baffle and the second fin

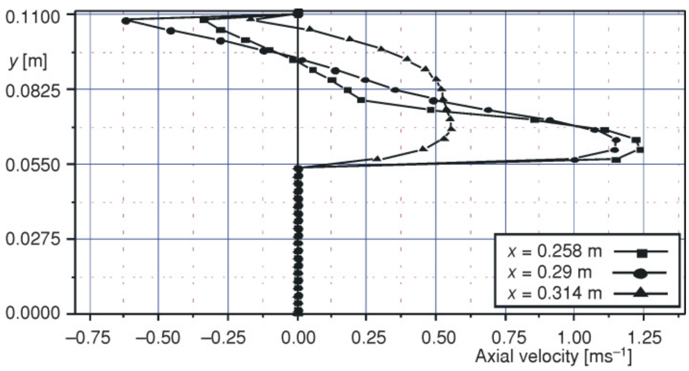

Figure 7. Velocity profiles between the first fin and the second baffle

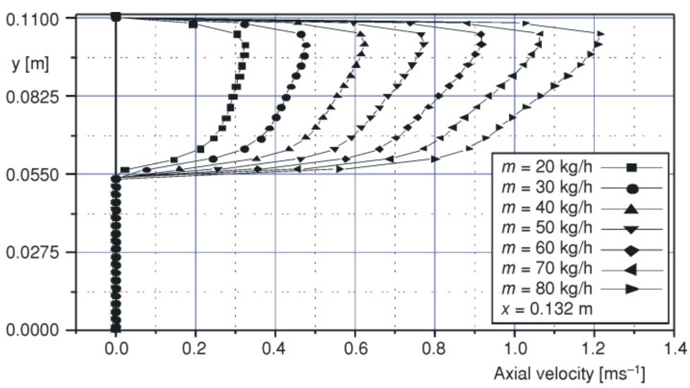

Figure 8. Effect of the mass flow rate on the axial velocity profiles upstream of first baffle

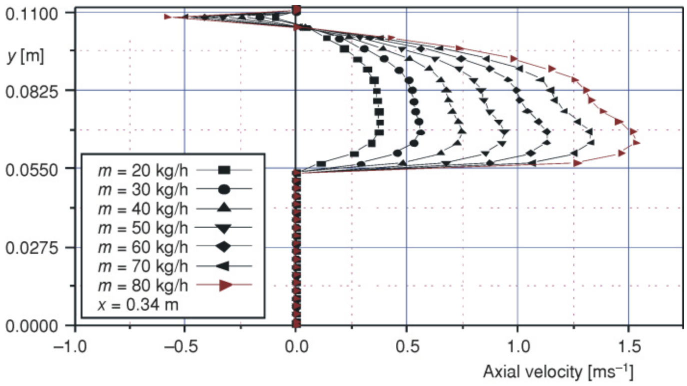

Figure 9. Effect of the mass flow rate on the axial velocity profiles upstream of second baffle

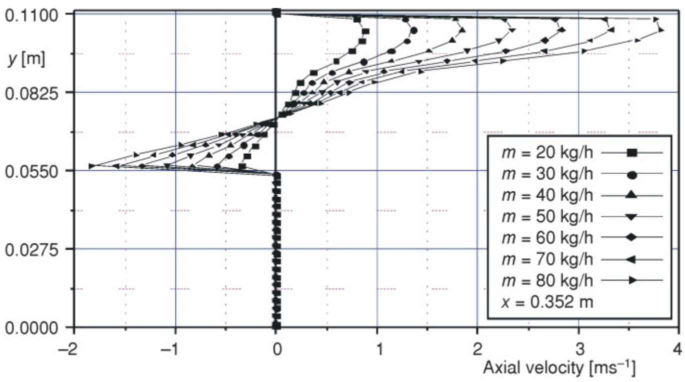

Figure 10. Effect of the mass flow rate on the axial velocity profiles between the second baffle and the second fin (x = 0.352 m)

fer from the surface of the absorbing plate to the following air.

Heat transfer aspects

The temperature contours in the solar collector with baffles and fins are plotted in fig. 11. The plot shows that the fluid temperature in the vortex region is significantly high as compared to that in the same region of no baffle region. In the region downstream of the two baffles, recirculation cells with low temperature are observed. In the regions between the tip of the fins and the channel wall, the temperature is increased. Due to the changes in the flow direction produced by the presence of the singularity of obstacles, the highest temperature value appears behind the lower channel wall with an acceleration process that starts just after the first fin and the second baffle.

The temperature profiles in longitudinal sections of the solar collector are plotted in figs. 12 and 13 at the positions defined in figs. 6 and 7. By referring to the velocity distribution, the temperature gradient at the heated wall decreases with increasing the flow velocity. This is due to the fact that the appearance of the negative values of the velocity reduces the level of the turbulence intensity inside the boundary layer. The recirculating region

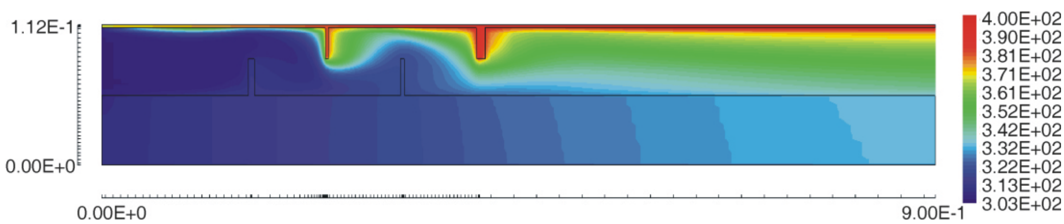

Figure 11. Temperature [K] distribution in the solar collector (m = 20 kg/h, L/B = 3/2, I_0 = 1043 W/m^2, ℓ = 16 cm) (color image see on our web site)

and the temperature lines are both restricted to the lower left corner of the baffle. The cold external air flows parallel along the bottom wall.

The fluid continues to be heated up along the duct proportionally to the number of baffles attached to the absorber. Further, for high flow rates, the collector operating temperature would be lower, figs. 14 and 15, resulting in lower heat losses and, consequently, higher efficiencies, fig. 16.

In term of efficiency, the fig. 16 shows the effect of mass flow rate on the performance of solar collector. As expected, it can be clearly observed that values of efficiency become higher with increasing values in the mass flow rate. This increment in the performances is caused by increasing the velocity of the flow. Also, the comparison between the solar collector with and without fins and baffle, according to the graphs of the efficiency, shows a noticeable improvement of the performances of the insulator provided with fins. Increase in efficiency due to the influence of fin is, also, a function of flow (for example for an air flow of 30 kg/h, one notes an increase of 15.5%).

Figure 16 show the thermal efficiency for different values of mass flow rate of air and for three categories of solar panel. It is observed that

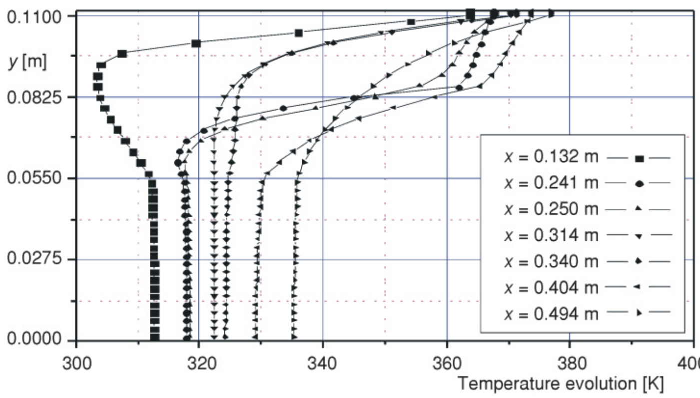

Figure 12. Temperature profiles in different sections of the solar collector (m = 30 kg/h, L/B = 3/2, I_0 =1043 Wm², e = 2 cm, ℓ = 16 cm)

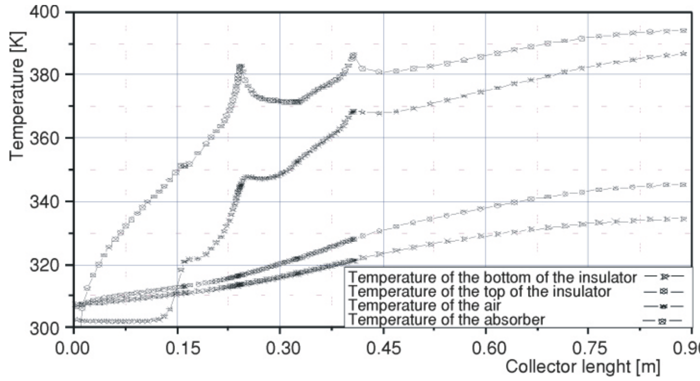

Figure 13. Temperature profiles in longitudinal sections of the solar collector

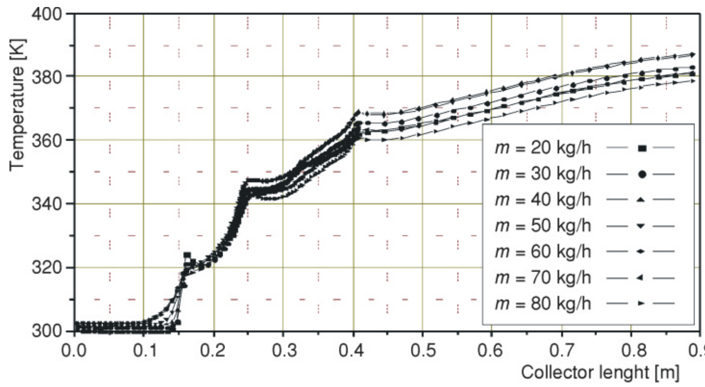

Figure 14. Mass flow rate effect on air temperature

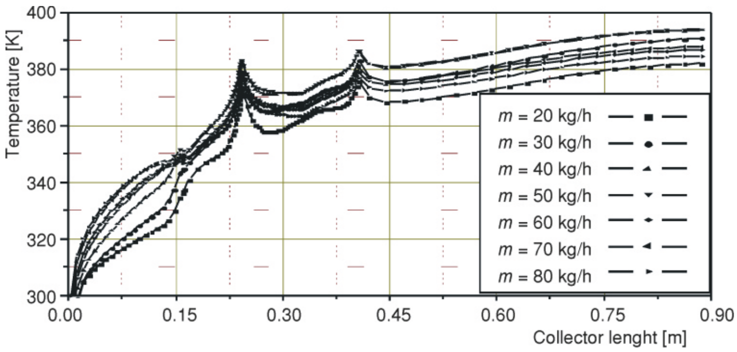

Figure 15. Mass flow rate effect on absorber plate temperature

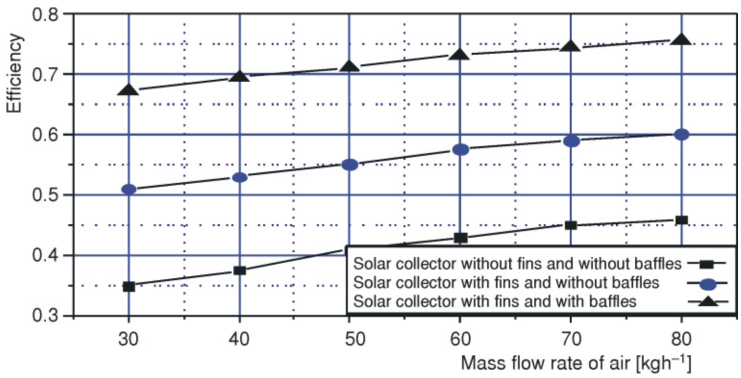

Figure 16. Efficiency of different solar collectors

the increase in the values of the efficiency are more significant for a collector provided with baffles and fins compared with those obtained for a solar collector without baffles and fins. It is clear that the thermal improvements are even more significant for low mass flow rates of air comparing with the high and average mass flow rates of air.

Conclusions

The present numerical study has focused on the investigation of forced convection and flow characteristics of a turbulent flow of air in a solar collector with fins and baffles inserts. The geometry of the problem is a simplification of the geometry found in solar collector with baffles and fins.

The numerical results obtained by this study have been validated by experimental results. The objective was to present an analysis of the dynamic and thermal comportment of turbulent flow using the k-ε model at low Reynolds number in a rectangular channel equipped with baffles and fins.

Profiles velocity distributions show a zone of recirculation relatively intense, over every aspect of baffles and fins, which moves downstream. The highest disturbance is obtained before the first fins. Finally, these vortex areas are responsible for variations of local heat transfer along the surfaces of fins and hot wall.

The results are reported for different mass flow rate and for different configurations of collectors. It was observed that the efficiency increases with the intensification of the volume flow rate in one hand and also increases with the presence of fins and baffles in other hand. However, increasing the air flow rate not only increases the pressure loss but also increases the fan power and, thereby, leads to increased operating cost. Consequently, a proper increase of the collector aspect ratio and proper installation of fins and baffles should be economically feasible in the design of a solar air heater.

Nomenclature

A_c – surface area of collector, LB, [m^2]
B – collector width, [m]
C_p – specific heat of air at constant pressure, [kJ kg^{-1}K^{-1}]
$C_{\varepsilon 1}$ – constant used in the standard k-ε model
$C_{\varepsilon 2}$ – constant used in the standard k-ε model
C_μ – constant used in the standard k-ε model
D – term which arises when low Reynolds number turbulence models are implemented
D_e – equivalent diameter of conduit, [m]
E_{LRN} – term which occurs when low Reynolds number (LRN) turbulence models are used
e – baffle height, [m]
f_1, f_2, f_μ – the modelling damping functions used for the LRN k-ε model
H – height of air tunnel in solar collector, [m]
h_w – convective heat transfer coefficient for air over outside surface of glass cover, [Wm^{-2}K^{-1}]
I_0 – incident solar radiation, [Wm^{-2}]
k – turbulent kinetic energy, [m^{2}s^{-2}]
L – collector length, [m]
L_1 – distance upstream of the first chicane, [m]
L_R – distance downstream of the second fin, [m]
m – mass flow rate of air, [kgs^{-1}]
n – co-ordinate normal to the wall, [–]
P – pressure, [Pa]
Pr – laminar Prandtl number, [–]
$\mathrm{Pr_t}$ – turbulent Prandtl number, [–]
P_k – a two-dimensional flow production term
Q_u – useful gain of energy carried away by air per unit time, [W]
Re – Reynolds number, [$U_{in}\nu/\lambda_f$], [–]
R_T, R_y – constants used in LRN k-ε model
t – time, [s]
T – temperature, [K]
T_a – ambient temperature, [K]
T_{in} – inlet temperature, [K]
U_{in} – inlet velocity, [ms^{-1}]
u, v – air velocity in the x, y direction, [ms^{-1}]
V – wind velocity, [ms^{-1}]
w_b – width of baffles, [m]
x – axial (along the wind tunnel axis), transversal
y – transversal co-ordinate (perpendicular to the wind tunnel axis)
y_L – width of the field of calculation, [m]
ℓ – distance between two baffles or two fins, [m]

Greek letters

δ_{absor} – thickness of absorber, [m]
δ_{isol} – thickness of insulator, [m]
ε – dissipation rate of turbulence energy, [m^{2}s^{-3}]
η – collector efficiency, [–]
κ – Von Karman constant (= 0.4)
λ_s, λ_f – thermal conductivity of solid, fluid – [Wm^{-1}K^{-1}]
λ_{isol}, λ_{absor} – thermal conductivity of insulator and absorber, respectively [Wm^{-1}K^{-1}]
μ, μ_t – laminar, turbulent viscosity, [Nsm^{-1}]
μ_e – effective viscosity, [Pa·s]
ν – kinematics viscosity, [m^{2}s^{-1}]
ρ – density of the air, [kgm^{-3}]
σ_ε – turbulent Prandtl number for ε, [–]
σ_k – turbulent Prandtl number for the turbulent kinetic energy, [–]
σ_T – turbulent Prandtl number for temperature
ϕ – stands for the dependent variables u, v, k, T, and ε

Subscripts and superscript

absor – absorber
e – effective
f – fluid
in, out – inlet, outlet of the test section
isol – insulator
t – turbulent

References

[1] Yang, Y., Hwang, C. Z., Calculation of Turbulent Flow and Heat Transfer in a Porous-Baffled Channel, *International Journal of Heat and Mass Transfer, 46* (2003), 5, pp. 771-780
[2] Patankar, S. V., Liu, C. H., Sparrow, E. M., Fully Developed Flow and Heat Transfer in Ducts Having Streamwise-Periodic Variation of Cross-Sectional Area, *J. of Heat Transfer, 99* (1977), 2, pp. 180-186
[3] Kelkar, K. M., Patankar, S. V., Numerical Prediction of Flow and Heat Transfer in Parallel Plate Channel with Staggered Fins, *Journal of Heat Transfer, 109* (1987), 1, pp. 25-30

[4] Berner, C., Durst, F., McEligot, E. M., Numerical Study of Fluid Flow and Heat Transfer in a Parallel Plate Channel with Baffles, *Journal of Heat Transfer, 106* (1984), 4, pp. 743-754
[5] Webb, B.W., Ramadhyani, S., Conjugate Heat Transfer in a Channel with Staggered Ribs, *International Journal of Heat and Mass Transfer, 28* (1985), 9, pp. 1679-1687
[6] Lopez, J. R., Anand, N. K., Fletcher, L. S., Heat Transfer in a Three-Dimensional Channel with Baffles, *Numerical Heat Transfer, 30* (1996), 2, pp. 189-205
[7] Cheng, C. H. , Huang, W. H. , Numerical Prediction for Laminar Forced Convection in Parallel-Plate Channels with Transverse Fin Arrays, *International Journal of Heat and Mass Transfer, 34* (1991), 11, pp. 2739-2749
[8] Founti, M. A. , Whitelaw, J. H., Shell Side Flow in a Model Disc and Doughnut Heat Exchanger, Tech. Report FS/81/37, Mech. Eng. Dept., Imperial College, London, UK, 1981
[9] Berner, C., Durst,F., McEligot, D. M. , Flow Around Baffles, *Trans. ASME J. Heat Transfer, 106* (1984), 4, pp. 743-749
[10] Berner, C., Durst,F., McEligot, D. M., Streamwise-Periodic Flow Around Baffles, *Proceedings,* 2nd International Conference on Applications of Laser Anemometry to Fluid Mechanics, Lisbon, 1984, pp. I4-I5
[11] Habib, M. A., *et al*., Experimental Investigation of Heat Transfer and Flow over Baffles of Different Heights, *Trans. ASME Journal of Heat Transfer, 116* (1994), 2, pp. 363-368
[12] Bazdid-Tehrani, F., Naderi-Abadi, M., Heat and Fluid Flow in Entrance Region of a Channel with Staggered Baffles, *International Communication on Heat Mass Transfer, 31* (2004), 15-16, pp. 2011-2019
[13] Ackermann, J. A., Ong, L-E., Lau, S. C., Conjugate Heat Transfer in Solar Collector Panels with Internal Longitudinal Corrugated Fins – Part I: Overall Results, *Forschung in Ingenieurwesen, 61* (1995), 4, pp. 84-92
[14] Bhargava, A. K., Garg, H. P., Sharma, V. K., Evaluation of the Performance of Air Heaters of Conventional Designs, *Solar Energy , 29* (1982), 6, pp. 523-533
[15] Wijeysundera, N. E., Ah, L. L., Tjioe, L. E., Thermal Performance Study of Two Pass Solar Air Heaters, *Solar Energy, 28* (1982), 5, pp. 363-370
[16] Youcef-Ali, S., Study and Optimization of the Thermal Performances of the Offset Rectangular Plate Fin Absorber Plates, with Various Glazing, *Renewable Energy, 30* (2005), 2, pp. 271-280
[17] Youcef-Ali, S., Desmons, J.Y., Numerical and Experimental Study of a Solar Equipped with Offset Rectangular Plate Fin Absorber Plate, *Renewable Energy, 31* (2006), 13, pp. 2063-2075
[18] Moummi, N., Youcef-Ali, S., Moummi, A., Desmons, S., Energy Analysis of a Solar Air Collector with Rows of Fins, *Renewable Energy, 29* (2004), 13, pp. 2053-2064
[19] Jones, W. P., Launder, B. E., The Calculation of Low-Reynolds Number Phenomena with a Two-Equation Model of Turbulence, *International Journal Heat Mass Transfer, 16* (1981), 6, pp. 1119-1130
[20] Versteeg, H. K., Malalasekera, W., An Introduction to Computational Fluid Dynamics; The Finite Volume Method, Longman Scientific and Technical, London, 1995
[21] McAdams, W. H., Heat Transmission, 3rd ed., McGraw-Hill, New York, USA, 1954
[22] Capderou, M., Solar Atlas of Algeria: Energetic Aspect (in French), Vol. 2, Office des Publications Universitaires, Algeria, 1985
[23] Whillier, A., Solar Energy Collection and Its Utilization for House Heating, Ph. D. thesis, MIT, Cambridge, Mass., USA, 1953
[24] Hottel, H. C., Whillier, A., Evaluation of Flat Plate Collector Performance, Transaction of the Conference on the Use of Solar Energy, University of Arizona Press, Vol. 2, 1958, pp. 74-104
[25] Whillier, A., Applications of Solar Energy for Heating and Cooling of Buildings, *ASHRAE*, New York, 1977, pp. 27-40
[26] Patankar, S. V., Numerical Heat Transfer and Fluid Flow, Hemisphere Publ. Comp., Washington, DC, 1980
[27] Ben Slama, R., The Air Solar Collectors: Comparative Study, Introduction of Baffles to Favor the Heat Transfer, *Solar Energy, 81* (2007), 1, pp. 139-149
[28] Latif, M. J., Heat Convection, Springer-Verlag, Berlin Heidelberg, 2006

Paper submitted: February 7, 2009
Paper revised: February 28, 2009
Paper accepted: March 26, 2009